



PCCP

Product Detection Study of the Gas-phase Oxidation of Methylphenyl Radicals using Synchrotron Photoionisation Mass Spectrometry

Journal:	<i>Physical Chemistry Chemical Physics</i>
Manuscript ID	CP-ART-04-2019-001935.R1
Article Type:	Paper
Date Submitted by the Author:	08-Jul-2019
Complete List of Authors:	Prendergast, Matthew; University of Wollongong, School of Chemistry Kirk, Benjamin; University of Wollongong, ARC Centre of Excellence for Free Radical Chemistry and Biotechnology Savee, John; ABB Inc, R&D Osborn, David; Sandia National Laboratories, Taatjes, Craig; Sandia National Laboratories, Hemberger, Patrick; Paul Scherrer Institut, Swiss Light Source Blanksby, Stephen; Queensland University of Technology, Central Analytical Research Facility da Silva, Gabriel; The University of Melbourne, Chemical Engineering Trevitt, Adam; University of Wollongong, Chemistry

SCHOLARONE™
Manuscripts

Product Detection Study of the Gas-phase Oxidation of Methylphenyl Radicals using Synchrotron Photoionisation Mass Spectrometry

Matthew B. Prendergast,¹

Benjamin B. Kirk,¹

John D. Savee,² David L. Osborn,² Craig A. Taatjes,²

Patrick Hemberger³

Stephen J. Blanksby,⁴

Gabriel da Silva,⁵

Adam J. Trevitt^{1}*

Authors' affiliations:

1. School of Chemistry, University of Wollongong, Wollongong NSW 2522, Australia.
2. Combustion Research Facility, Sandia National Laboratories, Livermore CA 94551-0969, USA.
3. Laboratory for Femtochemistry and Synchrotron Radiation, Paul Scherrer Institut, CH-5232 Villigen PSI, Switzerland
4. Central Analytical Research Facility, Queensland University of Technology, Brisbane QLD 4001, Australia.
5. Department of Chemical and Biomolecular Engineering, The University of Melbourne, Melbourne VIC 3010, Australia

Abstract

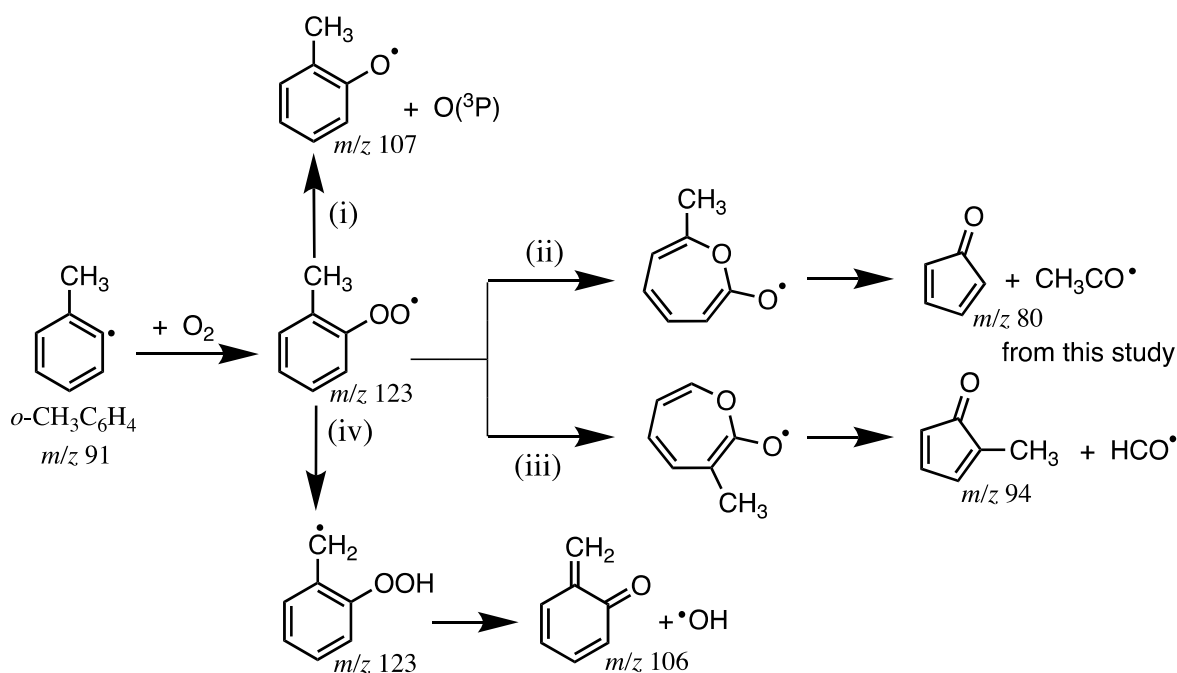
Product detection studies of the gas-phase oxidation of *o*-methylphenyl radicals and *m*-methylphenyl radicals are reported at ambient temperature (*ca.* 298 K) and 4 Torr (533.3 Pa) using VUV synchrotron photoionisation mass spectrometry. It is shown that cyclopentadienone (*c*-C₅H₄=O) + CH₃CO and *o*-quinone methide (*o*-CH₂=C₆H₄=O) + OH are unique product pathways to the *o*-methylphenyl + O₂ reaction due to mechanisms requiring the CH₃ group to be adjacent to the phenyl radical site. Common product pathways include methylphenoxy radical + O(³P) and isomers of methylcyclopentadienone (CH₃C₅H₄=O) + HCO. G3X-K quantum chemical calculations are deployed to rationalise experimental results for *o*-methylphenyl and *m*-methylphenyl radical oxidation. The *o*-quinone methide formation mechanism from *o*-methylphenyl + O₂ is analogous to formation of *o*-benzoquinone from *o*-hydroxyphenyl + O₂ where, after O₂ addition, the *ortho*-substituent in the phenylperoxyl intermediate undergoes a 1,5-H shift and eliminates OH. Other reaction products, including methylcyclopentadienone species and methylphenoxy radicals, are rationalised by applying known phenyl oxidation mechanisms. Transition state bifurcations are present in both radical systems and have exclusive end products (with different molecular mass). Compared to previous *o*-hydroxyphenyl and charged-tagged methylphenyl radical oxidation studies, there are significantly more products owing to the activation in this radical system and the competitiveness of rate limiting pathways.

1. Introduction

Toluene and other methylated benzenes, including xylenes, are added in significant quantities to gasoline as octane boosting agents because they inhibit autoignition in spark-ignition engines.¹ In high-temperature and combustion-related studies, methylated benzenes are subjected to H-atom abstraction by OH, and other radicals, and chemical models consider the production and fate of both methylphenyl and benzyl radicals.²⁻³ No direct detection of a methylphenyl radical within a combustion environment has been reported to our knowledge. The *o*-methylphenyl (*o*-CH₃C₆H₄) radical, also known as the *o*-tolyl radical, is implicated in the oxidation of *o*-xylene,⁴⁻⁶ and also in benzyl decomposition schemes.⁷⁻⁸

The barrier for isomerisation of *o*-CH₃C₆H₄ to benzyl has been calculated using the CBS-QB3 method at 43 kcal mol⁻¹ (180 kJ mol⁻¹) with a reverse barrier of 65 kcal mol⁻¹ (272 kJ mol⁻¹).⁹ Theoretical work on this reaction suggests that lifetimes for the *o*-CH₃C₆H₄ radical at temperatures less than 1000 K are sufficient for bimolecular reactions.¹⁰ Available O₂ could react with *o*-CH₃C₆H₄ radicals at temperatures relevant to low temperature combustion to form the *o*-methylphenylperoxy intermediate that promptly dissociates to free radical products.¹¹⁻¹² The benzyl radical, on the other hand, is notoriously unreactive to O₂.

Reactions of *m*-methylphenyl (*m*-CH₃C₆H₄) and *p*-methylphenyl (*p*-CH₃C₆H₄) with O₂ result in formation of *m*- and *p*-methylphenoxy + O(³P),¹³⁻¹⁵ which can be understood by applying “phenyl-like” oxidation mechanisms,¹⁶⁻¹⁸ *i.e.*, the methyl group is essentially a spectator to the reaction. The cross molecular beam study of the *p*-methylphenyl radical + O₂ reported at a collision energy of 35.3 kcal mol⁻¹ reported a single product channel forming via a complex-formation mechanism leading to the formation *p*-methylphenoxy radical + O(³P).¹⁵ As with the phenyl + O₂ reaction, the formation of methyloxepinoxy radicals are expected at lower temperatures (<900 K). These two pathways, direct O(³P) atom loss and oxepinoxy formation, are shown as pathways (i), (ii), and (iii) in Scheme 1 for the *o*-CH₃C₆H₄ case, where pathways (ii) and (iii) implicate two methyloxepinoxy isomers. Five-member rings (*in blue*) extending from pathways (ii) and (iii) in Scheme 1 are introduced in the present study. Pathway (iv) is proposed as a *major* pathway under low temperature conditions and is unique to the *ortho*-substituted case.^{11, 19-20}



Scheme 1. Major reaction pathways for the *o*-methylphenyl (*o*- $CH_3C_6H_4$) reaction with O_2 .

A previous experimental study of the trimethylammonium-methylphenyl radical cation oxidation,¹⁹ a distonic radical-ion analogue for *o*- $CH_3C_6H_4 + O_2$, provided direct experimental evidence supporting the *o*-quinone methide + OH pathway (pathway (iv) in Scheme 1) proposed by da Silva *et al.*¹¹ The mechanism is similar to that reported recently by our group for *o*-hydroxyphenyl + O_2 , which forms *o*-benzoquinone + OH *via* a QOOH-like phenoxyl radical intermediate.²⁰ This mechanism analogous of the Waddington mechanism for the decomposition of β -hydroxyperoxyl radicals towards OH loss.²¹⁻²⁴

In this present study, we report the gas-phase oxidation experiments of *o*- $CH_3C_6H_4$ and *m*- $CH_3C_6H_4$ radicals using synchrotron-based multiplexed photoionisation mass spectrometry (PIMS).²⁵⁻²⁶ The reactions of both *o*- and *m*- $CH_3C_6H_4$ radicals result in numerous products with two major differences: the detection of m/z 80 and 106 ions from *o*- $CH_3C_6H_4 + O_2$. Electronic structure calculations reveal competition between pathways (ii), (iii) and (iv) for *o*- $CH_3C_6H_4 + O_2$ while an analogous pathway (iv) for *m*- $CH_3C_6H_4 + O_2$ is inaccessible.

2. Experimental

2.1 Multiplexed Photoionisation Mass Spectrometry

The methylphenyl + O₂ reactions were investigated using multiplexed PIMS²⁵⁻²⁶ with synchrotron radiation from the Chemical Dynamics Beamline²⁷⁻²⁹ at the Advanced Light Source (ALS) synchrotron, Lawrence Berkeley National Laboratory (USA). The apparatus consists of a quartz slow-flow tube reactor, differentially pumped vacuum chamber, and an orthogonal acceleration time-of-flight mass spectrometer with VUV synchrotron photoionisation (PI).

Photolysis of either *o*-iodotoluene or *m*-iodotoluene was performed with a pulsed KrF excimer laser (248 nm) operating at 4 Hz and a fluence of approximately 50 mJ cm⁻² to generate the corresponding *o*-CH₃C₆H₄ or *m*-CH₃C₆H₄ radicals within the reactor *via* C–I bond homolysis. The quartz reactor is 62 cm long with an internal diameter of 1.05 cm and is maintained at 4 Torr (533.3 Pa) and ambient temperature.

Gas is continuously effused from the reactor into a surrounding differentially pumped vacuum chamber through a 650 μm diameter pinhole situated 37 cm along the flow tube. The effused gas is sampled by a skimmer to create a near-effusive molecular beam that is intersected by quasi-continuous undulator VUV synchrotron radiation. Ions generated by PI at this point are sampled using a 50 kHz pulsed orthogonal-acceleration time-of-flight mass spectrometer.

The VUV synchrotron PI energy is typically scanned from 8.00 to 10.20 eV in 0.025 eV steps. Mass spectra are compiled into three-dimensional arrays as functions of mass-to-charge, reaction time, and PI energy. Background subtraction of the ion signal is performed by recording signal 20 ms prior to the 248 nm photolysis pulse and subtracting the average of that signal from the post-laser signal. All data presented herein are normalised for variations in the ALS photon flux using a NIST-calibrated photodiode (SXUV-100, International Radiation Detectors Inc.).

PI spectra are obtained by integrating each mass peak over kinetic time and plotting the result as a function of VUV photon energy. The resulting PI spectra are then normalised to an integrated area of one and averaged with error bars representing two standard deviations (2σ) for an average of at least three measurements. The absolute PI cross sections for many species assigned in this investigation are unknown; consequently, a quantitative comparison of product yields could not be performed. Kinetic traces provided in the Supporting Information are obtained by integrating a *m/z* signal over PI energies (or at a set PI energy) and plotting the result as a function of reactor kinetic time.

Iodotoluene entrained in He with the optional addition of O₂ were supplied to the reactor through separate mass-flow controllers at a total rate of 102 sccm. Iodotoluene vapour was entrained in He by passing He through a fritted bubbler that contained liquid *o*-iodotoluene kept at 20 °C (293 K) and 470 Torr (62.7 kPa) or *m*-iodotoluene at 20 °C (293 K) and 364 Torr (48.5 kPa). *o*-Iodotoluene (98%) and *m*-iodotoluene (99%) were purchased from Sigma Aldrich. Vapour pressures were approximated using Antoine parameters for *o*-iodotoluene.³⁰ In experiments with *o*-iodotoluene at 298 K and 4 Torr, number densities within the reactor were approximately 1.1×10^{13} molecule cm⁻³ *o*-iodotoluene, 2.5×10^{16} molecule cm⁻³ O₂, and a total of 1.3×10^{17} molecule cm⁻³ including the He buffer gas. In the case of *m*-iodotoluene, at 298 K and 4 Torr the number densities were approximately 1.1×10^{13} molecule cm⁻³ *m*-iodotoluene, 1.3×10^{16} molecule cm⁻³ O₂, and a total of 1.3×10^{17} molecule cm⁻³ He gas.

2.2 Threshold Photoelectron spectroscopy

Pyrolysis measurements on *o*-methylanisole (*o*-CH₃C₆H₄OCH₃) were performed at the X04DB (VUV) beamline³¹ of the Swiss Light Source (SLS) at Paul Scherrer Institut in Switzerland. An approximately 0.1% mixture of *o*-methylanisole (*o*-CH₃C₆H₄OCH₃) in argon with a flow rate of 50 sccm was expanded through a 100 μm pinhole into a pyrolytic microreactor (internal diameter = 1 mm), which can be heated up to 1500 K. The gas mixture leaving the reactor forms a molecular beam where reactive intermediates are not quenched. Based on the paper of Guan *et al.*,³² we have estimated the residence time and pressure in the reactor to 100 μs and 10-40 mbar, respectively. After skimming (2 mm) the beam, the sampled gas reaches the ionization region of the CRF-PEPICO spectrometer³³⁻³⁴ and is ionised by VUV synchrotron radiation from the SLS storage ring. Ions and electrons are velocity map imaged and detected by delay line anode detectors in coincidence using the multiple-start multiple stop approach.³⁵ Photoion mass-selected threshold photoelectron spectra (ms-TPES) are obtained by scanning the photon energy and correlating threshold electrons (near zero kinetic energy) with coincident ions. Hot electrons are treated using the approach by Sztáray *et al.*³⁶ PI spectra are recorded by plotting the ion signal in coincidence with all kinetic energy electrons correlated with the species of interest.

2.3 Quantum Chemical Calculations

Adiabatic ionisation energies (AIEs) reported in electron volts (eV) were calculated with the CBS-QB3 composite method³⁷⁻³⁸ using Gaussian09.³⁹ To rationalise mechanisms for generation of detected products, enthalpies of key reaction intermediates and transition states were calculated for *o*-CH₃C₆H₄ + O₂ and *m*-CH₃C₆H₄ + O₂ using the G3X-K method.⁴⁰ The relative reaction enthalpies are reported in kcal mol⁻¹ relative to the reactants. Reported enthalpies and AIEs incorporate the zero-point (0 K) energy correction.

3. Results and Discussion

3.1 Photolysis Products of *o*-Iodotoluene and *m*-Iodotoluene

As initial baseline measurements, product mass spectra from 248 nm photolysis of *o*-iodotoluene or *m*-iodotoluene without O₂ added to the flow reactor were recorded and are provided as Figure S1 in the Supporting Information. The major product peaks at *m/z* 90 and 92 are assigned to fulvenallene (c-C₅H₄=C=CH₂)⁴¹ and toluene,⁴² respectively, by comparing experimental PI spectra to reference spectra. The production of fulvenallene is attributed to HI loss as a photolysis product of iodotoluene, an additional photoproduct channel to methylphenyl + I, similar to HBr loss observed from *o*-bromophenol.⁴³ In the absence of oxygen, the detection of toluene is attributed to subsequent H-atom abstraction by methylphenyl radicals from abundant iodotoluene in the flow. At these photolysis energies (248 nm corresponds to 115 kcal mol⁻¹) no isomerisation between the *m*-CH₃C₆H₄ and *o*-CH₃C₆H₄ is expected as the isomerisation barrier is calculated¹⁰ to be 62 kcal mol⁻¹ and using the iodobenzene C—I bond energy from Ref. 44 to approximate the iodotoluene C—I bond energy leaves 48 kcal mol⁻¹, which is well below the isomerisation barrier energy. The *o*-CH₃C₆H₄ to benzyl radical isomerisation barrier is calculated¹⁰ at 43 kcal mol⁻¹ so some minor *o*-CH₃C₆H₄ to benzyl isomerisation might be possible.

3.2 Detection of the Oxidation Products from *o*-CH₃C₆H₄ and *m*-CH₃C₆H₄ Radicals

Figure 1a and Figure 1b are product mass spectra from 248 nm photolysis of *o*-iodotoluene and *m*-iodotoluene, respectively, with O₂ added to the flow. These mass spectra are integrated over 0–80 ms after photolysis (where 0 ms coincides with the firing of the photolysis laser) and acquired with a VUV

photon energy of 10.2 eV, with the reactor tube at room temperature. Isomerisation of thermalised methylphenyl radicals to the more stable benzyl radical at temperatures <1000 K is calculated to be negligible.¹⁰ Compared with the baseline measurements (Figure S1), all major new product ion signals (*i.e.*, not m/z 90 and 92) in Figure 1 are attributed to methylphenyl + O₂ reactions.

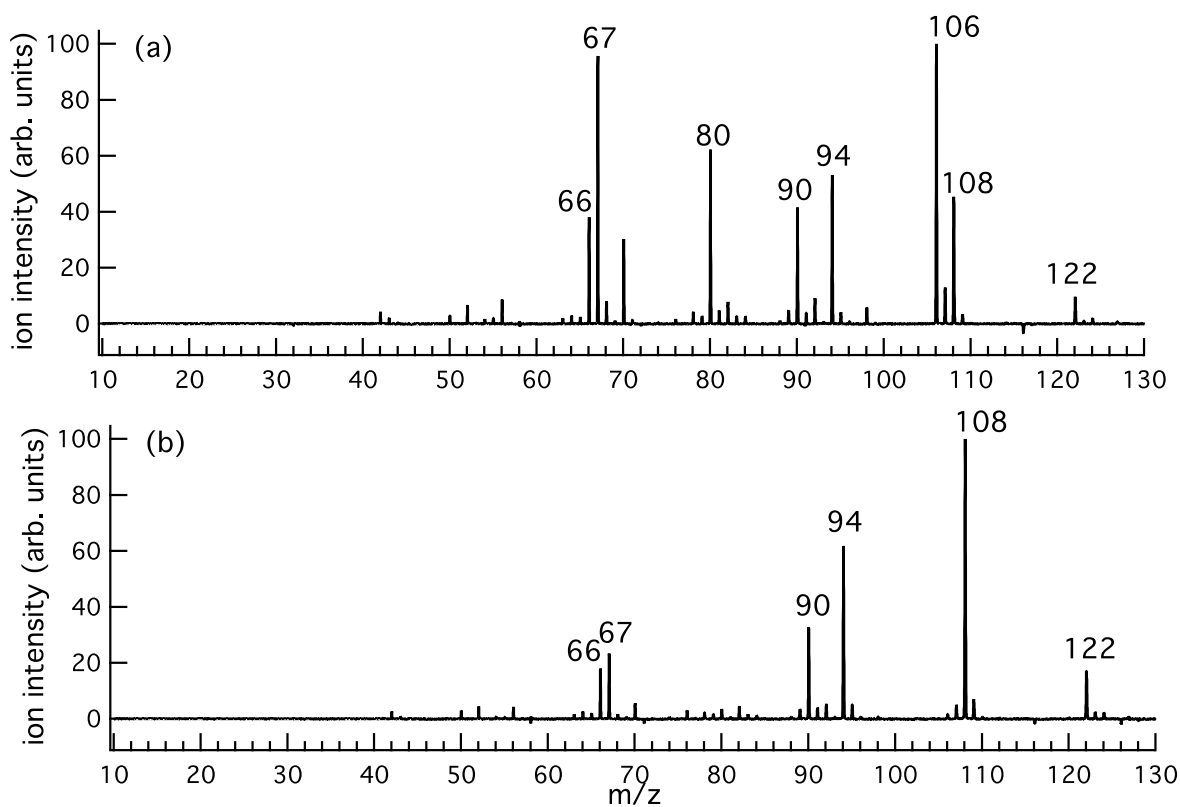


Figure 1. Product mass spectra at 10.2 eV integrated 0–80 ms after 248 nm photolysis of (a) *o*-iodotoluene and (b) *m*-iodotoluene in the presence of O₂ at room temperature.

As evident from Figure 1a and Figure 1b, the major oxidation product signals are present at m/z 66, 67, 70, 80, 94, 106, 107, 108, and 122. Notable differences between *o*-CH₃C₆H₄ + O₂ (Figure 1a) and *m*-CH₃C₆H₄ + O₂ (Figure 1b) are that m/z 80 and 106 ion signals are significant in the *o*-CH₃C₆H₄ case but absent in the *m*-CH₃C₆H₄ case. Also, the m/z 67 ion intensity is significantly diminished for *m*-CH₃C₆H₄ (Figure 1b) compared to *o*-CH₃C₆H₄ case (Figure 1a) while the inverse is true for m/z 108 signal. Overall, the product chemistry is surprisingly rich, especially when compared to our recent study on the oxidation of *o*-hydroxyphenyl where only two major products were observed.²⁰

The combination of PIMS with tuneable synchrotron radiation²⁵⁻²⁶ provides a means to record PI spectra by monitoring photo-ion signal intensity as a function of photon energy. The onset and shape of PI spectra can be used to identify reaction products with isomeric specificity by comparison to reference or calculated PI spectra. Quantifying product branching fractions usually requires knowledge of the absolute PI cross section; unfortunately, the absolute PI cross sections for many products relevant to these *o*- and *m*-CH₃C₆H₄ + O₂ reactions are unknown and this prohibits quantitative comparison of product yields.

Figure 2 shows the PI spectrum for *m/z* 106, from *o*-CH₃C₆H₄ + O₂. The onset at 8.75 eV agrees with the calculated AIE at 8.7 eV for *o*-quinone methide (*o*-CH₂=C₆H₄=O). The *o*-CH₂=C₆H₄=O species is reactive⁴⁵⁻⁴⁶ and therefore, it is not straightforward to obtain a reference PI spectrum from a pure sample. Thus we have synthesized *o*-CH₂=C₆H₄=O *in situ* by pyrolysis of *o*-methylanisole in a microreactor and utilised photoelectron photoion coincidence (PEPICO) techniques on the X04DB (VUV) beamline at the Swiss Light Source (SLS) to record a PI spectrum. Figure 2 shows this PI spectrum of the coincident *m/z* 106 ions with a pyrolysis reactor temperature of around 1100 K.

To substantiate that this spectrum is in fact due to *o*-CH₂=C₆H₄=O, the threshold photoelectron spectrum (TPES), shown in Figure S2 of the Supporting Information, is first assigned. The TPES shows two features at 8.76 and 9.32 eV, which agree with the conventional PE spectrum of Eck *et al.*⁴⁷ A Franck Condon analysis from (TD)-DFT geometries and force constant matrixes revealed contributions from both the ground and first excited-state of the *o*-CH₂=C₆H₄=O ion to the experimental TPE spectrum. It has been shown in the past that the combination of experimental and simulated TPE spectra is a suitable technique to isomer-selectively assign reactive intermediates in the gas-phase chemical reactions.⁴⁸⁻⁵⁰ A detailed analysis of the vibrational structure and assignment of the transitions will be forthcoming in a later publication. The PI spectrum of *o*-CH₂=C₆H₄=O, a spectrum of all collected electrons at each photon energy, is also obtained and is compared to the ALS PI spectrum of *m/z* 106 using the photolysis reactor setup (Figure 2). There is very good agreement between 8.8 and 9.5 eV confirming the assignment of *o*-CH₂=C₆H₄=O. The small offset deviation present below 8.8 eV in the SLS experiment is due to the low-pressure expansion at the exit of the reactor such that vibrational modes are not efficiently cooled and a T_{vib} of ~500 K can easily remain in the molecule. This leads to a significant hot and sequence band contribution⁵¹⁻⁵² that contributes to the small baseline offset between 8.4 and 8.7 eV. The mismatch above 9.5 eV is explained by reduction in detection efficiency of energetic ($E_{\text{kin}} > 1\text{ eV}$) electrons which are not fully imaged on the electron detector, which reduces ion counts in the coincidence detection scheme. The good agreement between 8.8 to 9.5 eV suggests that *p*-quinone methide (*p*-CH₂=C₆H₄=O, AIE = 9.2 eV)

is not present. Another stable isomer is benzaldehyde (C_7H_6O , AIE = 9.5 eV)⁵³⁻⁵⁴, along with other isomers listed with their AIEs in Table S1 (Supporting Information), can be excluded based on the following investigation of the m/z 106 ion signal.

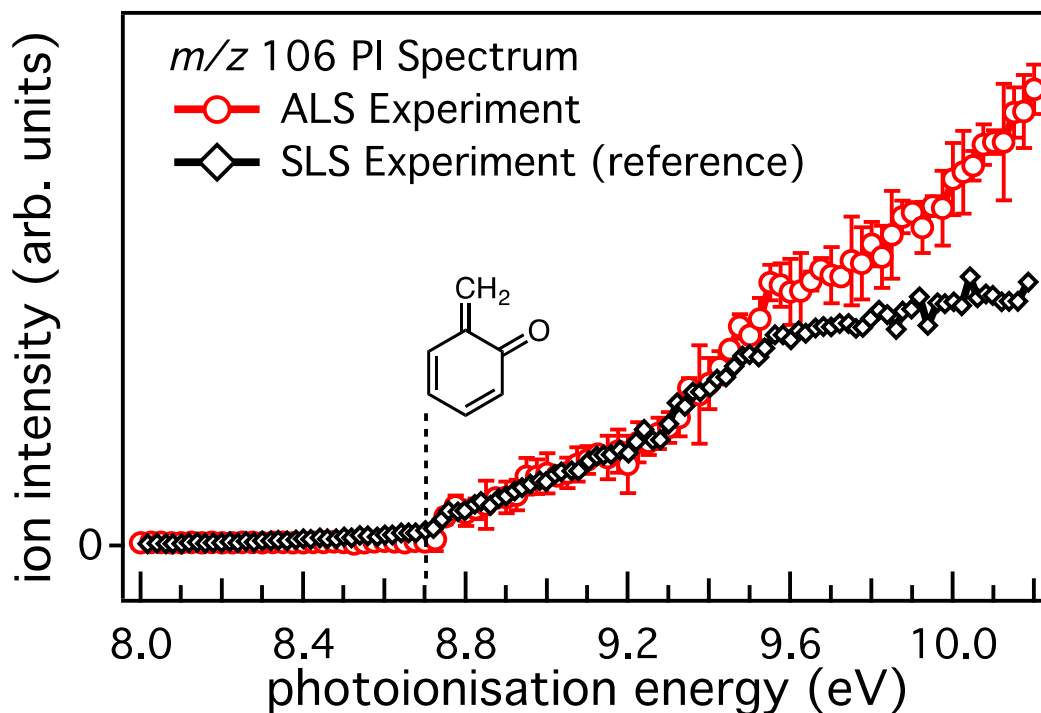


Figure 2. PI spectrum for m/z 106 from $o\text{-CH}_3\text{C}_6\text{H}_4 + \text{O}_2$ at ambient temperatures (red circles) integrated 0–80 ms after photolysis. The PI spectrum for the m/z 106 product from pyrolysis of o -methylanisole conducted at the SLS (black diamonds), as described in the main text.

To check further if the m/z 106 signal over 8.75–10.2 eV may be the result of multiple isomers, the m/z 106 product kinetics were examined at PI energies before and after the deviation at 9.5 eV between the traces in Figure 2. Figure S3 in the Supporting Information compares kinetic traces for m/z 106 integrated between 8.8–9.2, 9.4–9.8, and 9.8–10.2 eV. After formation, the m/z 106 ion signal decay profiles are all very similar, all with a distinct slow decay. This lends support to just one dominant m/z 106 isomer contributing to the PI spectrum from $o\text{-CH}_3\text{C}_6\text{H}_4 + \text{O}_2$. Ultimately, our explanation of the m/z 106 PI spectrum is that $o\text{-CH}_2=\text{C}_6\text{H}_4=\text{O}$ is the dominant isomer detected.

A mechanism describing the formation of $o\text{-CH}_2=\text{C}_6\text{H}_4=\text{O}$ from $o\text{-CH}_3\text{C}_6\text{H}_4 + \text{O}_2$ has been reported previously¹¹ and will be described in detail later (Section 3.3). The key pathway for the formation of $o\text{-CH}_2=\text{C}_6\text{H}_4=\text{O}$ is O_2 addition to $o\text{-CH}_3\text{C}_6\text{H}_4$ radical forming the $o\text{-CH}_3\text{C}_6\text{H}_4$ peroxy radical where the proximity of the methyl group facilitates a 1,5-H atom shift to the peroxy moiety and subsequent OH elimination from the QOOH intermediate.⁵⁵ Experimental studies into the oxidation of distonic $o\text{-CH}_3\text{C}_6\text{H}_4$ radical ions support the proposed mechanism.¹⁹ This pathway is unlikely for $m\text{-CH}_3\text{C}_6\text{H}_4 + \text{O}_2$ as the same H-atom shift would require substantial deformation of the aromatic ring.

Moving to other products, Figure 3 shows the $o\text{-CH}_3\text{C}_6\text{H}_4 + \text{O}_2$ m/z 80 PI spectrum along with reference PI spectra for cyclopentadienone ($c\text{-C}_5\text{H}_4=\text{O}$, AIE = 9.41 eV) obtained from the literature.⁵⁶⁻⁵⁷ There is a good match to the m/z 80 ion signal and therefore this signal is conclusively assigned to cyclopentadienone. As shown later, the formation of cyclopentadienone is rationalised via a 7-methyloxepinoxyl radical intermediate that follows from O_2 addition. This cyclopentadienone product is formed by elimination of the acetyl radical (CH_3CO) following a mechanism that appears unique to the o -methylphenyl oxidation reaction (*cf.* the presence and absence of m/z 80 in Figures 1a and 1b, respectively). The m/z 80 product is absent from the $m\text{-CH}_3\text{C}_6\text{H}_4 + \text{O}_2$ reaction and this will be explained below following discussion of the computational results.

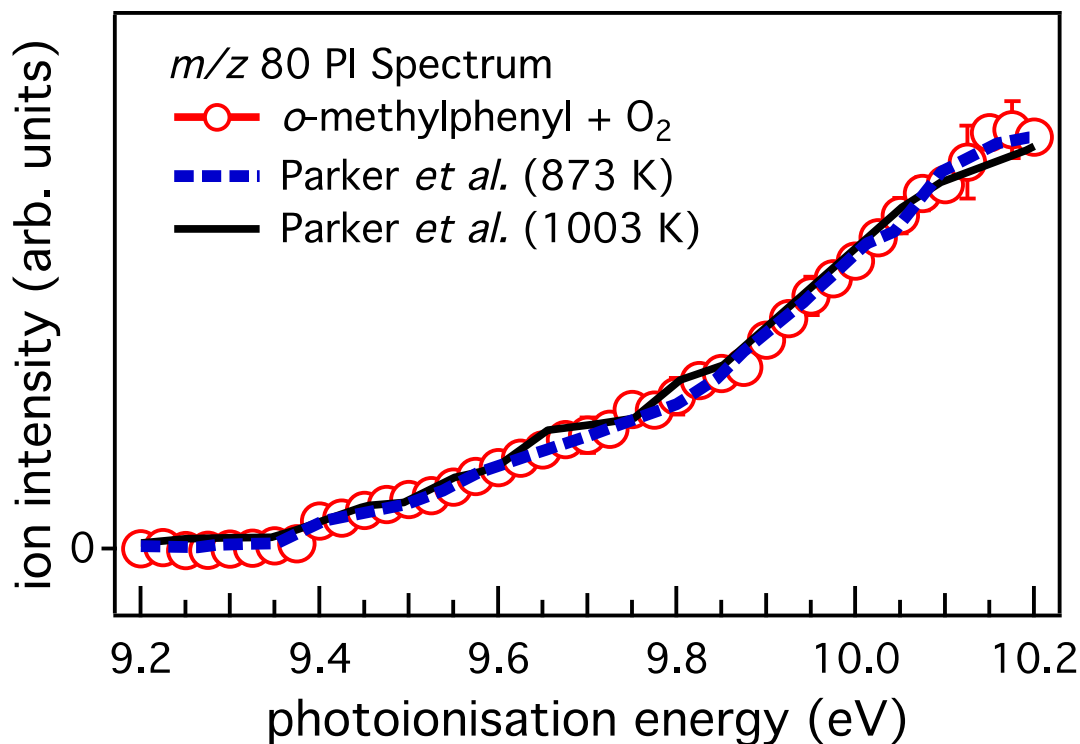


Figure 3. PI spectrum for m/z 80 from o -CH₃C₆H₄ + O₂ (open circles) integrated 0–80 ms after photolysis. PI spectra for cyclopentadienone (Parker et al.)⁵⁷ at 873 K (dotted blue line) and 1003 K (solid black line) are shown.

The m/z 94 signal is present in product mass spectra from both o - and m -CH₃C₆H₄ + O₂ (Figure 1a and Figure 1b) and PI spectra of this product are presented in Figure S4. These traces appear matched near the onset region 8.85 eV but deviate beyond 9.10 eV. The onset at 8.85 eV excludes the presence of phenol as a significant contributor to ion signal because the phenol ionisation energy is lower at 8.508 ± 0.001 eV.^{54, 58} The 8.85 eV onset is consistent with the calculated AIE for 2-methylcyclopentadienone (AIE = 8.9 eV). The deviation near 9.0 eV aligns with the PI onset of 3-methylcyclopentadienone (AIE = 9.1 eV), which is unique to the m -CH₃C₆H₄ + O₂ reaction as will be outlined below.

Figure S5 shows the m/z 108 PI spectrum from the o -CH₃C₆H₄ and m -CH₃C₆H₄ + O₂ reactions that shows reasonable agreement with the previously reported PE spectrum for m -cresol⁵⁹ (m -CH₃C₆H₄OH) between 8.2–9.2 eV. An inflection near 9.9 eV is consistent with features present within integrated PE spectra for cresols⁵⁹ but also aligns with the PI onset for p -benzoquinone (AIE = 9.96 ± 0.01 eV).^{54, 60-61} The 7–12 eV PE spectra reported for the cresol isomers o -CH₃C₆H₄OH, m -CH₃C₆H₄OH, and p -CH₃C₆H₄OH and these have generally similar PI onsets and spectral features, particularly between 8–10.2 eV,⁵⁹ which frustrates any disentanglement of individual cresol isomers. However, in this study any cresol formation has to be rationalised as a non-primary product channel due to the number of hydrogen atoms. In these reactions it is likely that, following O₂ addition to the CH₃C₆H₄ radical, loss of O(³P) from the peroxy adduct leads to formation of the methylphenoxy radical (m/z 107). It is this methylphenoxy radical that presumably abstracts a H-atom from another species in the gas flow and forms a cresol as a secondary product. To support this idea, the fitted first-order rate coefficients for appearance of m/z 108 ion signal from o - and m -CH₃C₆H₄ + O₂ reactions are fitted to be 500 ± 70 (1 σ) s⁻¹ and 400 ± 20 (1 σ) s⁻¹, respectively (shown in Figure S6), which are significantly lower values than the 3000 ± 1000 (1 σ) s⁻¹ and 2600 ± 400 (1 σ) s⁻¹ appearance rates for m/z 107 from o - and m -CH₃C₆H₄ + O₂ (integrated over the 8.0–10.2 eV photon energy range), respectively. The m/z 107 signal is too weak to interpret the PI spectrum. The calculated AIEs of the two relevant methylphenoxy radicals, listed in Table S2, are consistent with a m/z 107 PI observed onset values at roughly > 8.3 eV. The relatively large and small rate coefficients for

appearance of m/z 107 and 108, respectively, are consistent with a primary reaction to produce a phenoxy radical and secondary H-atom abstraction to produce cresols that dominate the m/z 108 ion signal between 8.0–10.0 eV.

On the possible formation of *o*-benzoquinone ($o\text{-O}=\text{C}_6\text{H}_4=\text{O}$, AIE = 9.2 eV, m/z 108), we have shown in a previous study²⁰ that at PI energies >9.8 eV, $o\text{-O}=\text{C}_6\text{H}_4=\text{O}$ undergoes dissociative ionisation *via* loss of CO to form m/z 80.²⁰ A boost in m/z 80 PI signal at photon energies >9.8 eV can signify the presence of $o\text{-O}=\text{C}_6\text{H}_4=\text{O}$. The PI spectrum of m/z 80 here in Figure 3 is compared to our previous work where $o\text{-O}=\text{C}_6\text{H}_4=\text{O}$ dissociative ionisation affected the m/z 80 PI spectrum (from *o*-hydroxyphenyl + O₂ experiments)²⁰ this comparison is shown in Figure S7. The absence of any enhancement in m/z 80 ion signal at PI energies >9.8 eV, coupled with the good agreement with m/z 80 PI spectra included in Figure S7 from Ref. 57, suggests that $o\text{-O}=\text{C}_6\text{H}_4=\text{O}$ is not present in major amounts, perhaps not at all.

The m/z 122 PI spectrum in Figure S8 from $o\text{-CH}_3\text{C}_6\text{H}_4 + \text{O}_2$ features a gradual PI onset around 8.6 eV followed by an abrupt rise in signal near 9.75–9.85 eV. There is weak signal between 8.6–9.6 eV for the $o\text{-CH}_3\text{C}_6\text{H}_4$ case where the $m\text{-CH}_3\text{C}_6\text{H}_4 + \text{O}_2$ result is at the background level. Pathways to reaction products, including methyl-substituted benzoquinone, formed via methyloxepinoxy intermediates, are considered in reaction schemes described below (see Figures 7, 8, and 9). However, the species contributing to the m/z 122 PI spectra in Figure S8 appear to be secondary products based on a fitted appearance rate of $\sim 200 \text{ s}^{-1}$ between 0–10 ms at 10.2 eV. This rate is slower than the appearance rate of m/z 108 signal (Section 3.2.4) and thus we suspect that this m/z 122 signal is not a primary reaction product. The AIEs for a range of C₇H₆O₂ isomers were calculated and listed in Table S3. The hydroxy-1,2-quinone methide and methide oxepinone isomers are unlikely to be present because their AIEs are <8.6 eV. Other isomers in Table S3 have calculated AIEs between 8.6–10.2 eV and 2-hydroxy-benzaldehyde is the most stable by approximately 20–30 kcal mol⁻¹. The weak m/z 122 signal, and absence of a reference PI spectra for plausible assignments, leaves the m/z 122 product ion signal unassigned but is not likely to be a primary reaction product.

From both methylphenyl radical + O₂ reactions there are peaks present in both Figure 1a and Figure 1b at m/z 66, 67, and 70 that are consistent with C₅H₆, C₅H₇, and C₄H₆O, respectively. For $o\text{-CH}_3\text{C}_6\text{H}_4 + \text{O}_2$, the ions appear at a kinetic growth rate of $1500 \pm 300 \text{ s}^{-1}$ for m/z 66, $510 \pm 40 \text{ s}^{-1}$ for m/z 67, and $1000 \pm 100 \text{ s}^{-1}$ for m/z 70. When compared to the appearance of m/z 80 ($1100 \pm 200 \text{ s}^{-1}$), assumed to be a good

reference pseudo first-order rate constant for a primary reaction product, these inverse time constants suggest that m/z 66 and 70 are primary reaction products and m/z 67 is not. Pathways to these lighter products were not investigated in further detail here. Since the activation of the methyloxepinoxyl radical from methylphenyl + O₂ is considerable – approaching 100 kcal mol⁻¹ – there are many pathways that are thermodynamically possible.

3.3 Computational Investigation of *o*-CH₃C₆H₄ + O₂ and *m*-CH₃C₆H₄ + O₂

Potential energy schemes were calculated using the G3X-K method⁴⁰ in order to guide the interpretation of experimental results and comparisons between the *o*- and *m*-CH₃C₆H₄ + O₂ systems. All reaction enthalpies are reported in kcal mol⁻¹ relative to the respective entrance channel (***o1*** for *o*-CH₃C₆H₄ + O₂ and ***m1*** for *m*-CH₃C₆H₄ + O₂).

A potential energy scheme for *o*-CH₃C₆H₄ + O₂ (***o1***) (Figure 4) follows the major pathways identified by da Silva *et al.*¹¹ The *o*-methylphenylperoxy radical (***o2***, -47.3 kcal mol⁻¹) can undergo: dissociation back to *o*-CH₃C₆H₄ + O₂ (***o1***), homolytic O–O bond cleavage resulting in O(³P) loss with *o*-methylphenoxy radical formation (***o3***), isomerisation to either 3- or 7-methyl-oxepinoxyl radicals (***o5***, ***o6***, respectively) *via* a bifurcated region of the reaction surface,^{17, 62} or a intramolecular 1,5-H-atom shift between the adjacent methyl and peroxy substituents with subsequent OH loss to form *o*-CH₂=C₆H₄=O (***o8***). Figure 5 shows a similar potential energy schematic for decomposition of *m*-methylphenylperoxy (***m2***) with the notable exception that OH formation pathway is absent. The H-atom shift followed by OH loss, which is important for the *ortho*-case (*i.e.*, ***o2*** → ***o3*** → ***o8***), is not accessible for the *meta*-case because the methyl-to-peroxy H-atom transition state is >50 kcal mol⁻¹ above the reactants (***m1***), compared to -19.9 kcal mol⁻¹ in the *o*-CH₃C₆H₄ + O₂ reaction. “Our calculations of the O₂ addition energy and O atom elimination pathways for the *meta*- and *ortho*-system are in accord with Ref. 15 for the *p*-CH₃C₆H₄ radical using the G3(MP2,CC)//B3LYP/6-311++G(d,p) method. They are listed here, respectively, for the O₂ addition energy and O (³P) reaction pathway product energy: *ortho*: -47 kcal mol⁻¹, -11 kcal mol⁻¹; *meta*: -47 kcal mol⁻¹, -9 kcal mol⁻¹; *para*: -46 kcal mol⁻¹, -10 kcal mol⁻¹.”

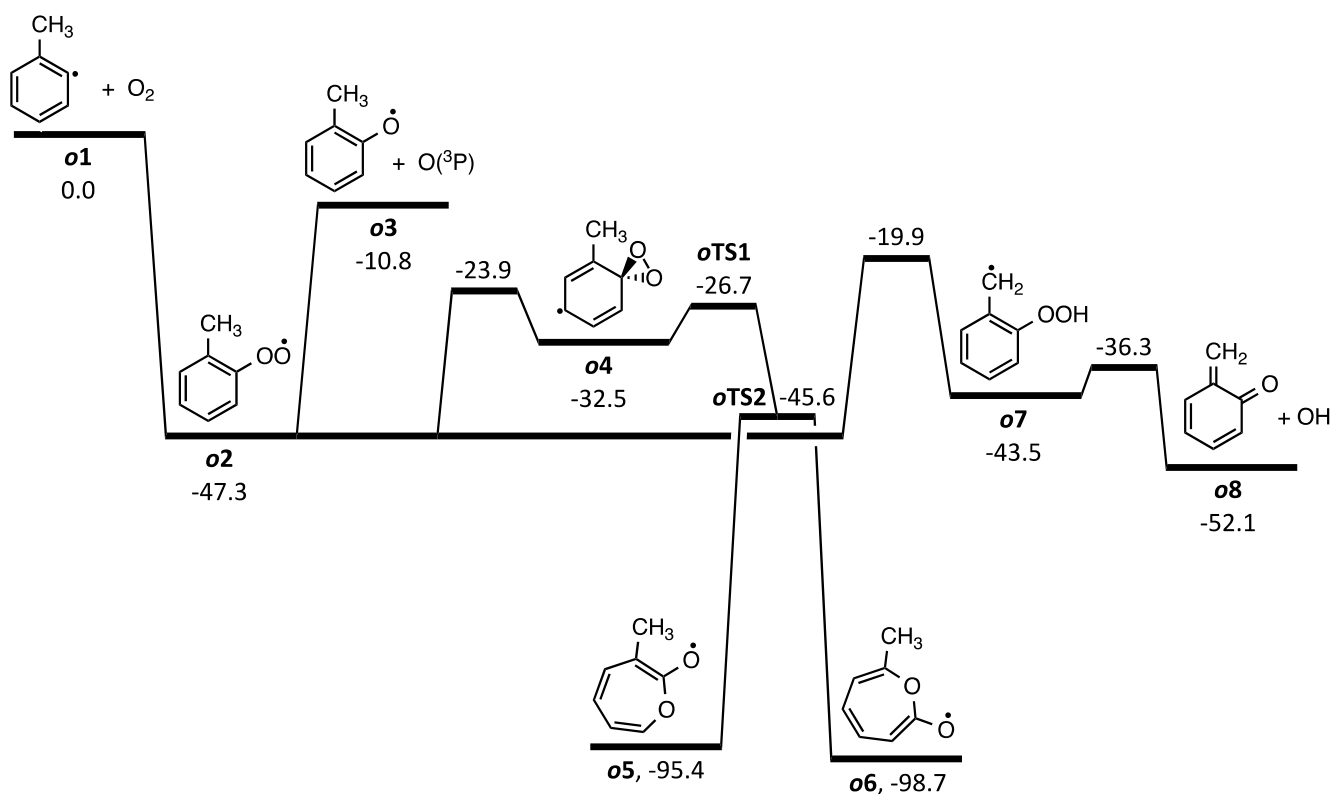


Figure 4. Potential energy scheme for the *o*-methylphenyl + O₂ reaction. The transition state **oTS1** leads to a bifurcation point on the potential energy surface (**oTS2**), which connects to the methyl-oxepinoxyl radical isomers **o5** and **o6**. G3S-K 0 K enthalpies are reported in kcal mol⁻¹ relative to **o1**.

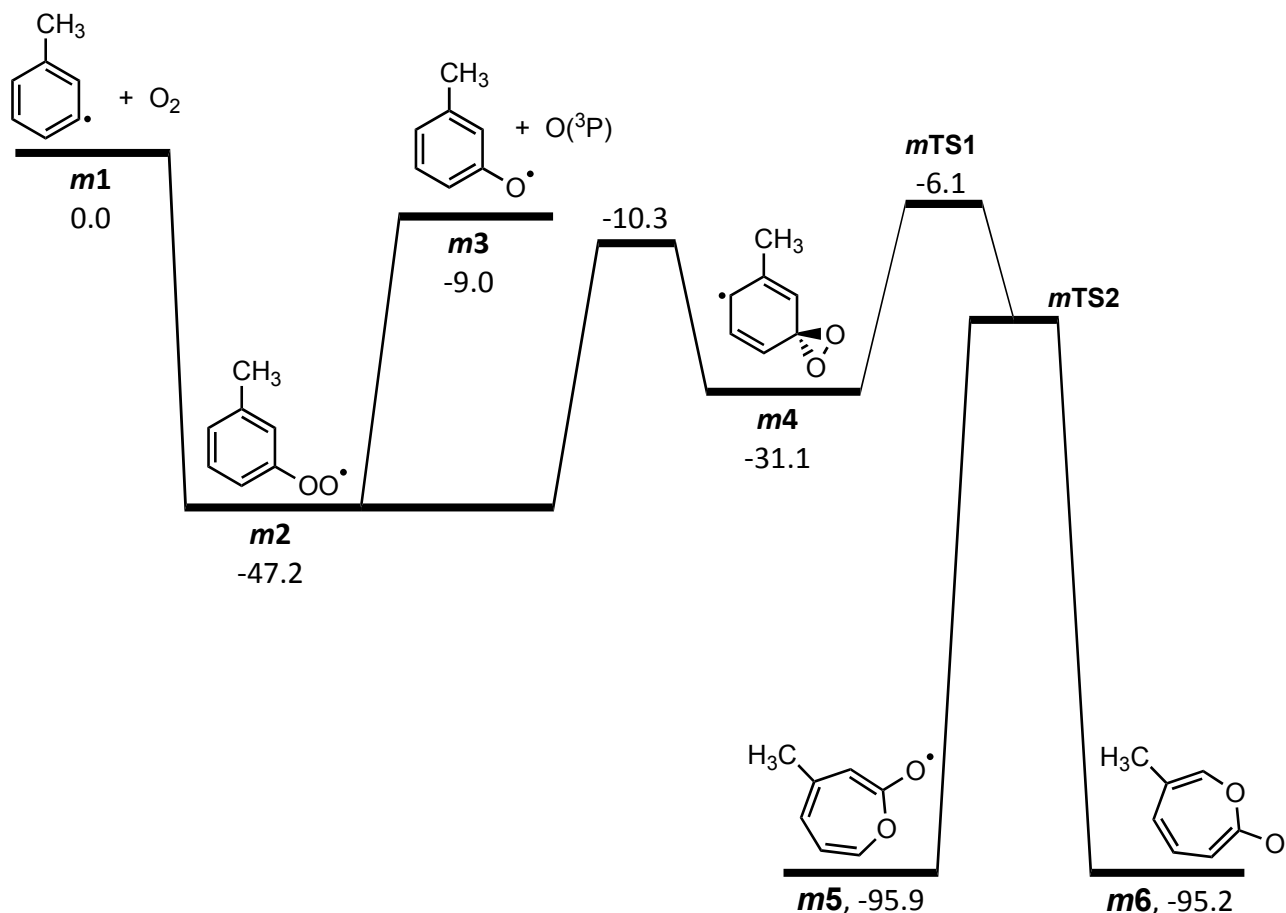


Figure 5. Potential energy scheme for the *m*-Mh + O₂ reaction. The transition state ***mTS1*** leads to a bifurcation point on the potential energy surface (***mTS2***), which connects to the methyl-oxepinoxyl radical isomers ***m5*** and ***m6***. G3S-K 0 K enthalpies are reported in kcal mol⁻¹ relative to ***m1***.

Figure 4 shows three reaction pathways for the *o*-CH₃C₆H₄ + O₂ reaction. All proceed through relatively similar reaction barrier heights and all reside considerably below the reactant energy. We conclude that all three processes are competitive and all are required to explain the experiments. Following the peroxy radical (***o2***), the pathway that bifurcates to the 3- and 7-methyloxepinoxyl radicals is predicted to be the lowest energy pathway overall. Here the most significant barrier is for initial *ipso* attack of the peroxy group at the aromatic ring to yield ***o4***, which still takes place at 23.9 kcal mol⁻¹ below the reactants. Following this, ***o4*** proceeds through ***oTS1***, which curiously connects to another first order saddle point, ***oTS2***, which is the isomerisation transition state between the 3- and 7-methyloxepinoxyl radicals. This represents a bifurcation point^{16-17, 62} on the potential energy surface, which mediates the reaction pathway between the two methyloxepinoxyl radicals. Although this same bifurcation mechanism is available to

the archetypal phenyl + O₂ reaction, with identical outcomes in that case, the methylphenyl result can be traced through to distinct reaction products as discussed further below.

An alternative reaction pathway, slightly higher in energy than oxepinoxyl formation, is the production of *o*-CH₂=C₆H₄=O + OH, which forms via the 1,5-H shift transition state (19.9 kcal mol⁻¹ below the reactants) and *o*-CH₂=C₆H₄=O detected in the experiments (Figure 2). The absence of the *m/z* 106 product signal for the *m*-CH₃C₆H₄ + O₂ reaction reveals that this pathway is distinctive to the *ortho*-radical case.

The direct O–O bond homolysis leading to O atom formation (at 10.8 kcal mol⁻¹ below the reactants) is also predicted to be significant pathway. This yields the *o*-methylphenoxy radical + O(³P), which we have assigned in the experimental results to be a significant product channel on the basis of indirect detection related to the detection of the *o*-cresol product observed at *m/z* 108, as explained above.

A potential energy scheme for the *m*-CH₃C₆H₄ + O₂ reaction is shown in Figure 5 and it resembles that of the *o*-CH₃C₆H₄ + O₂ reaction except for the absence of a OH elimination channel (*cf.* **o8**, Figure 4). The *m*-methylphenoxy + O(³P) product pathway is predicted to have the lowest barrier at -9.0 kcal mol⁻¹. Barriers along the oxepinoxyl pathway **mTS1** and **mTS2** are rather high when compared to the *ortho*-case (and higher than the bare phenyl case), which may be an artefact of spin contamination issues in the stationary point calculations and likely require further investigation. T1 diagnostic values⁶³ for both *ortho* and *meta* radical stationary points TS1 and TS2, and the O₂ peroxy radical adducts, are provided as Table S4 in the supporting information. The T1 diagnostic values for the TS1 and TS2 structure for both systems are significantly above 0.03 indicating multireference wavefunction issues and these states will require further examination with appropriate multiconfiguration approaches. The ROO adducts in both cases have T1 diagnostic values near 0.02. Nevertheless, both pathways are predicted to proceed well below the reactant energy.

The subsequent pathways for all the methyl-oxepinoxyl radicals are provided in Figures 6 and 7 for the *ortho*-reaction and Figures 8 and 9 for the *meta* reaction. Because of the sizable exothermicity of the oxepinoxyl formation (> 90 kcal mol⁻¹), many dissociation channels will be energetically feasible. Figures 6 to 9 illustrate the major channels we have identified guided by our experimental observations, but we cannot rule out other pathways that may be relevant and contributing to minor product present in the product mass spectra. For 7-methyl-oxepinoxyl (**o6**, Figure 6), the lowest energy dissociation channel

leads to cyclopentadienone (m/z 80) + CH_3CO , whereas the 3-methyl-oxepinoxyl (**o5**, Figure 7) leads to 2-methylcyclopentadienone (m/z 94) + HCO . Recall that both m/z 80 and 94 products are detected in the $o\text{-CH}_3\text{C}_6\text{H}_4 + \text{O}_2$ experiments. This therefore might represent a rare case in which a set of reaction products are controlled by a potential energy surface bifurcation where cyclopentadienone originates uniquely from **o6** and 2-methylcyclopentadienone uniquely from **o5**. We note that since we do not have photoionisation cross-section values for these species, we cannot conclude on their product branching fractions. Further work in quantifying these production pathways could provide valuable insight into the kinetics through bifurcated transition states.

There are alternative pathways for these oxepinoxyl radicals, these include isomerization to form either 1,2-benzoquinone (m/z 108) + CH_3 as shown in Figure 6, or 3-methyl-1,2-benzoquinone (m/z 122) + H as shown in Figure 7. Neither of these products are conclusively assigned as primary product. The small peak at m/z 122 is assigned as a secondary product based on kinetics arguments and the m/z 108 signal to not attributed to benzoquinone but to a side reaction (as detailed above).

For the $m\text{-CH}_3\text{C}_6\text{H}_4 + \text{O}_2$ reaction there are two relevant oxepinoxyl species (**m5** and **m6**) that lead to two isomeric forms of methylcyclopentadienone with HCO elimination, making bifurcation control less obvious. But, these pathways do appear to be divergent with **m5** leading to 3-methylcyclopentadienone (Figure 8) and **m6** leading to 2-methylcyclopentadienone (Figure 9). The overall major differences between the $o\text{-CH}_3\text{C}_6\text{H}_4$ and $m\text{-CH}_3\text{C}_6\text{H}_4$ reactions with O_2 are the formation of $o\text{-CH}_2=\text{C}_6\text{H}_4=\text{O}$ (m/z 106) and cyclopentadienone (m/z 80) products, which are unique to the $o\text{-CH}_3\text{C}_6\text{H}_4 + \text{O}_2$ reaction. While the lack of the $o\text{-CH}_2=\text{C}_6\text{H}_4=\text{O}$ product for the $m\text{-CH}_3\text{C}_6\text{H}_4 + \text{O}_2$ reaction is well explained at this point, the exclusivity of the cyclopentadienone product requires further discussion. In Figures 8 and 9, it is shown that the **m5** and **m6** pathways lead to methylcyclopentadienone products, with evidence for both detected in the $m\text{-CH}_3\text{C}_6\text{H}_4 + \text{O}_2$ results (Figure S4). The lack of cyclopentadienone is explained by comparing the fate of **o6.1** in Figure 6, where the crucial aspect is the location of the CH_3 group, with the corresponding **m5.1** and **m6.1** intermediates in Figures 8 and 9. The **o6.1** radical can ring close to a five-member ring by expelling the $-\text{COCH}_3$ group to position 2 on the ring (intermediate **o6.5**), setting up the radical directed elimination of CH_3CO and forming cyclopentadienone. For the corresponding **m5.1** and **m6.1** radicals, the CH_3 group is not in a position to be combined with CO to form the $-\text{COCH}_3$ leaving group and, therefore, only HCO radicals are eliminated. Thus there are crucial differences between the reaction products *ortho* and *meta* isomers of these methylphenyl radicals.

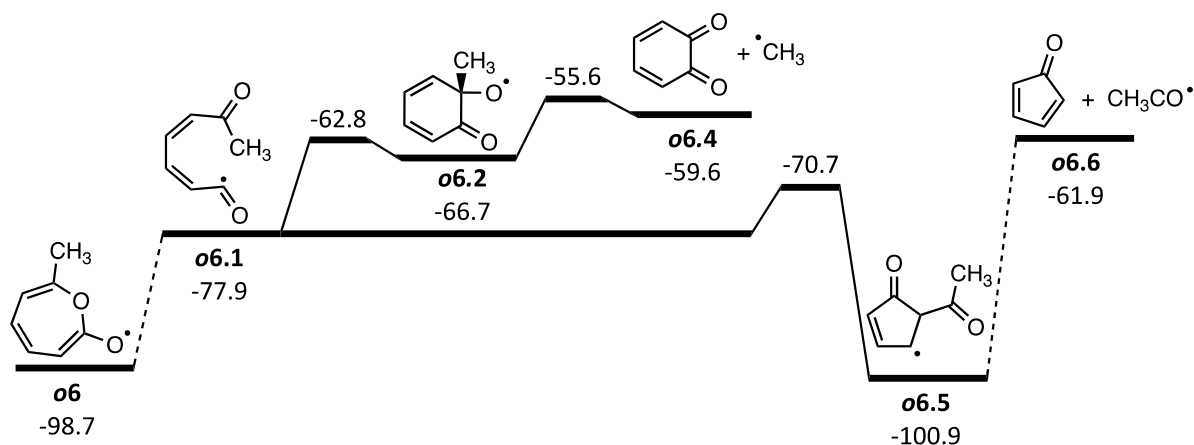


Figure 6. Potential energy schematic for decomposition of the 7-methyl-oxepinoxyl radical (**o6**) from isomerisation of **o2**. G3X-K 0 K enthalpies are reported in kcal mol⁻¹ relative to **o1**.

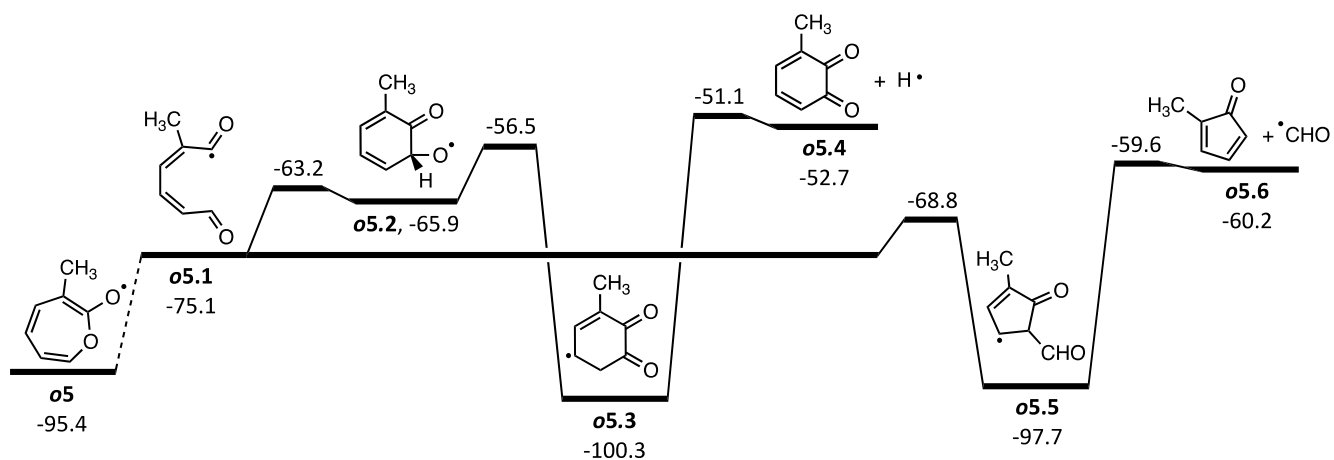


Figure 7. Potential energy schematic for decomposition of the 3-methyl-oxepinoxyl radical (**o5**) from isomerisation of **o2**. G3X-K 0 K enthalpies are reported in kcal mol⁻¹ relative to **o1**.

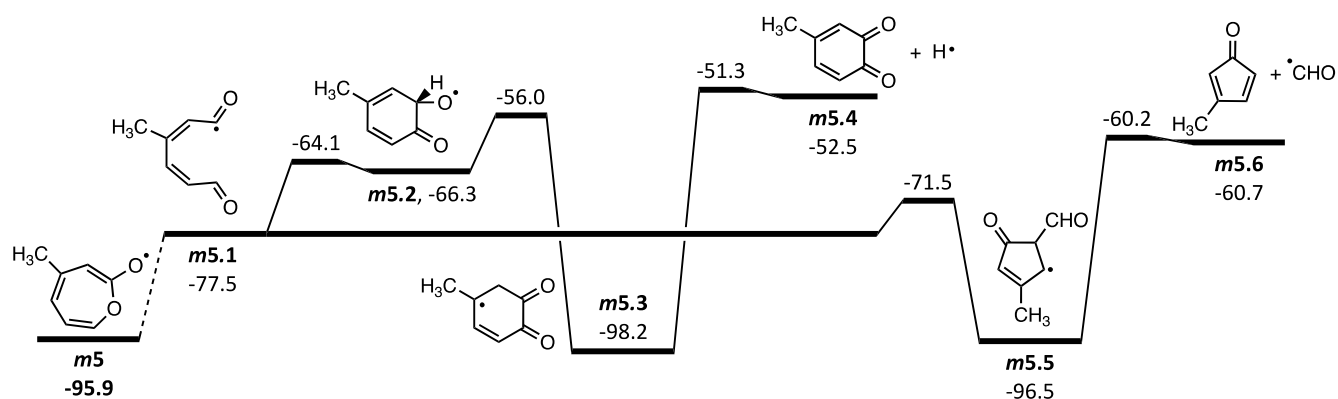


Figure 8. Potential energy scheme showing the decomposition of 4-methyloxepinoxyl (**m5**) from isomerisation of **m2**. G3X-K 0 K enthalpies are reported in kcal mol⁻¹ relative to **m1**.

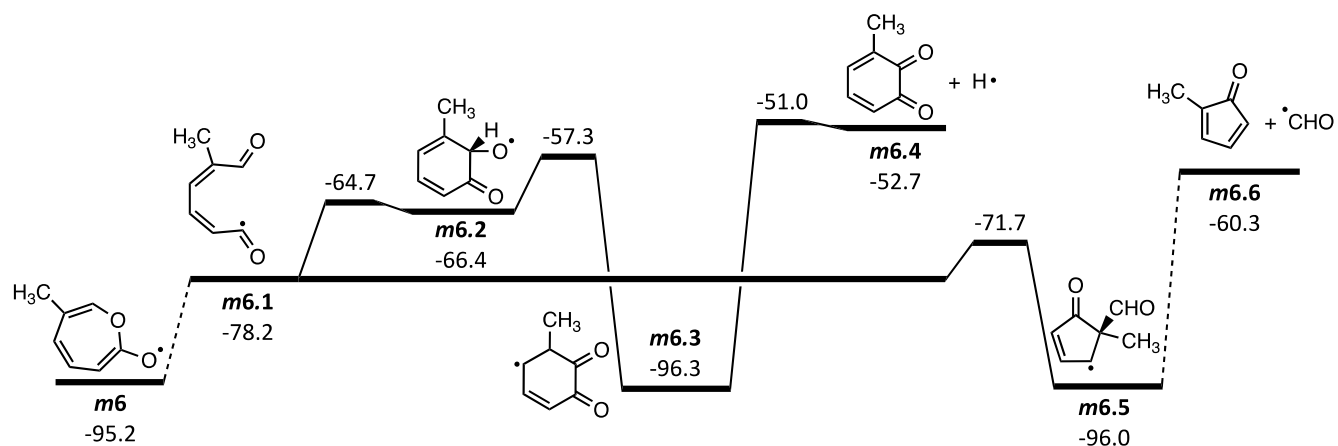


Figure 9. Potential energy scheme showing the decomposition of 6-methyloxepinoxyl radical (**m6**) from isomerisation of **m2**. G3X-K 0 K enthalpies are reported in kcal mol⁻¹ relative to **m1**.

4. Conclusion

Experiments conducted at the ALS synchrotron using multiplexed PIMS reveal extensive products from the *o*- and *m*-CH₃C₆H₄ + O₂ reactions. It is shown that the *m/z* 80 and 106 products are unique to the *o*-CH₃C₆H₄ case due to exclusive reaction pathways requiring the CH₃ group *ortho* to the radical site. The *m/z* 106 signal is assigned as *o*-quinone methide (*o*-CH₂=C₆H₄=O) based on comparison to PI spectra of *o*-CH₂=C₆H₄=O produced from a pyrolysis source using complementary experiments at the SLS. The formation mechanism for *o*-CH₂=C₆H₄=O upon oxidation of *o*-CH₃C₆H₄ is analogous to formation of *o*-*o*-O=C₆H₄=O + OH from *o*-hydroxyphenyl + O₂,²⁰ where the *ortho*-substituent participates in a 1,5-H

shift and subsequent OH elimination. The main difference between these two systems is that the rate-limiting barrier for the OH elimination from the peroxy radical adduct is significantly lower for *o*-hydroxyphenyl + O₂ (at ~10 kcal mol⁻¹) compared to 27 kcal mol⁻¹ for *o*-CH₃C₆H₄ + O₂. For *o*-hydroxyphenyl + O₂, under similar conditions, the *o*-benzoquinone + OH pathway is overwhelmingly dominant such that no other product pathway is detected. But for *o*-CH₃C₆H₄ + O₂, the higher barrier brings these other reaction pathways into play such that we see at least *six* distinct *m/z* product pathways. We note here also that the formation of an OH elimination product appears to be a general diagnostic for a O₂ reaction with suitable *ortho*-substituted phenyl radicals.^{19-20, 64}

Other reaction products are generally rationalised by applying an understanding of known phenyl oxidation mechanisms.¹⁷⁻¹⁸ Including pathways implicating methyl-substituted phenoxy and oxepinoxy radicals. Cyclopentadienone is formed from decomposition of the 7-methyloxepinoxy radical from *o*-CH₃C₆H₄ + O₂. Decomposition of 3-methyloxepinoxy radicals results in formation of 2-methylcyclopentadienone. In the *meta*-radical case, decomposition of 4- and 6-methyloxepinoxy radicals produces 2- and 3-methylcyclopentadienone, respectively. We note that these experiments are performed at room temperature and experiments at higher temperatures would need consider the likely rising dominance of the entropically favourable O-atom elimination channel.

These product detection experiments demonstrate the significant difference between the gas-phase reactivity of *ortho*- and *meta*-substituted aromatic radicals and furthermore the richness of aromatic oxidation chemistry.

6. Acknowledgements

The authors are grateful for the financial support of the Australian Research Council through the Discovery and Future Fellowship programs (DP170101596, DP140101237, DP130100862 and FT130101304). The authors also acknowledge the generous allocation of computing resources by the NCI National Facility (Canberra, Australia) under Merit Allocation Scheme. The participation of J.D.S., D.L.O., and C.A.T., and the development and operation of the MPIMS kinetics apparatus, are supported by the Office of Chemical Sciences, Geosciences, and Biosciences, Office of Basic Energy Sciences, United States Department of Energy. Sandia National Laboratories is a multi-mission laboratory managed and operated by National Technology and Engineering Solutions of Sandia, LLC, a wholly owned subsidiary of Honeywell International, Inc., for the U.S. Department of Energy's

National Nuclear Security Administration under contract DE-NA0003525. The Advanced Light Source is supported by the Director, Office of Science, Office of Basic Energy Sciences, of the U.S.

Department of Energy under Contract No. DE-AC02-05CH11231. This paper describes objective technical results and analysis. Any subjective views or opinions that might be expressed in the paper do not necessarily represent the views of the USDOE or the United States Government.

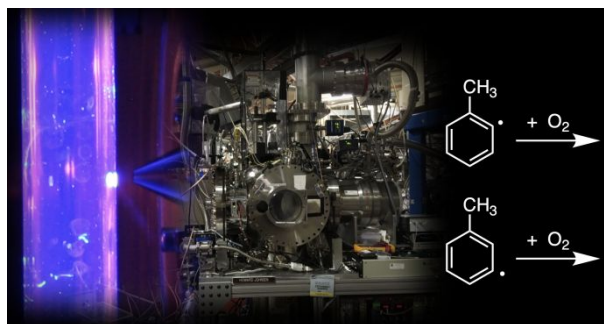
Pyrolysis experiments were performed at the VUV (X04DB) beamline of the Swiss Light Source located at Paul Scherrer Institute, Switzerland. P.H. acknowledges financial support by the Swiss Federal Office of Energy (SI/501269-01) and Patrick Ascher for technical support.

References

1. da Silva, G.; Bozzelli, J. W., *Combustion and Flame* **2010**, *157* (11), 2175-2183.
2. Seta, T.; Nakajima, M.; Miyoshi, A., *The Journal of Physical Chemistry A* **2006**, *110* (15), 5081-5090.
3. Li, Y.; Yuan, W.; Li, T.; Li, W.; Yang, J.; Qi, F., *Physical Chemistry Chemical Physics* **2018**, *20* (16), 10628-10636.
4. Battin-Leclerc, F.; Bounaceur, R.; Belmekki, N.; Glaude, P. A., *International Journal of Chemical Kinetics* **2006**, *38* (4), 284-302.
5. Narayanaswamy, K.; Blanquart, G.; Pitsch, H., *Combustion and Flame* **2010**, *157* (10), 1879-1898.
6. Wang, S.; Davidson, D. F.; Hanson, R. K., *Proceedings of the Combustion Institute* **2018**.
7. Shapero, M.; Cole-Filipiak, N. C.; Haibach-Morris, C.; Neumark, D. M., *The Journal of Physical Chemistry A* **2015**, *119* (50), 12349-12356.
8. Buckingham, G. T.; Porterfield, J. P.; Kostko, O.; Troy, T. P.; Ahmed, M.; Robichaud, D. J.; Nimlos, M. R.; Daily, J. W.; Ellison, G. B., *The Journal of Chemical Physics* **2016**, *145* (1), 014305.
9. Derudi, M.; Polino, D.; Cavallotti, C., *Physical Chemistry Chemical Physics* **2011**, *13* (48), 21308-21318.
10. Dames, E.; Wang, H., *Proceedings of the Combustion Institute* **2013**, *34* (1), 307-314.
11. da Silva, G.; Chen, C.-C.; Bozzelli, J. W., *The Journal of Physical Chemistry A* **2007**, *111* (35), 8663-8676.
12. da Silva, G.; Bozzelli, J. W., *The Journal of Physical Chemistry A* **2007**, *111* (32), 7987-7994.
13. Herbinet, O.; Husson, B.; Ferrari, M.; Glaude, P.-A.; Battin-Leclerc, F., *Proceedings of the Combustion Institute* **2013**, *34* (1), 297-305.
14. Bounaceur, R.; Da Costa, I.; Fournet, R.; Billaud, F.; Battin-Leclerc, F., *International Journal of Chemical Kinetics* **2005**, *37* (1), 25-49.
15. Thomas, A. M.; Yang, T.; Dangi, B. B.; Kaiser, R. I.; Kim, G.-S.; Mebel, A. M., *The Journal of Physical Chemistry Letters* **2016**, *7* (24), 5121-5127.
16. Carpenter, B. K., *Journal of the American Chemical Society* **1993**, *115* (21), 9806-9807.
17. Tokmakov, I. V.; Kim, G.-S.; Kislov, V. V.; Mebel, A. M.; Lin, M. C., *The Journal of Physical Chemistry A* **2005**, *109* (27), 6114-6127.
18. Sebbar, N.; Bockhorn, H.; Bozzelli, J., *International Journal of Chemical Kinetics* **2008**, *40* (9), 583-604.
19. Prendergast, M. B.; Cooper, P. A.; Kirk, B. B.; da Silva, G.; Blanksby, S. J.; Trevitt, A. J., *Physical Chemistry Chemical Physics* **2013**, *15*, 20577-20584.
20. Prendergast, M. B.; Kirk, B. B.; Savee, J. D.; Osborn, D. L.; Taatjes, C. A.; Masters, K.-S.; Blanksby, S. J.; da Silva, G.; Trevitt, A. J., *Physical Chemistry Chemical Physics* **2016**, *18*, 4320-4332.
21. Ray, D. J. M.; Redfearn, A.; Waddington, D. J., *Journal of the Chemical Society, Perkin Transactions 2* **1973**, (5), 540-543.
22. Ray, D. J. M.; Waddington, D. J., *Combustion and Flame* **1973**, *20* (3), 327-334.
23. Welz, O.; Zádor, J.; Savee, J. D.; Sheps, L.; Osborn, D. L.; Taatjes, C. A., *The Journal of Physical Chemistry A* **2013**, *117* (46), 11983-12001.
24. Silva, G. d.; Graham, C.; Wang, Z.-F., *Environmental Science & Technology* **2010**, *44* (1), 250-256.

25. Osborn, D. L.; Zou, P.; Johnsen, H.; Hayden, C. C.; Taatjes, C. A.; Knyazev, V. D.; North, S. W.; Peterka, D. S.; Ahmed, M.; Leone, S. R., *Review of Scientific Instruments* **2008**, *79* (10), 104103.
26. Savee, J. D.; Soorkia, S.; Welz, O.; Selby, T. M.; Taatjes, C. A.; Osborn, D. L., *The Journal of Chemical Physics* **2012**, *136* (13), 134307.
27. Suits, A. G.; Heimann, P.; Yang, X.; Evans, M.; Hsu, C. W.; Lu, K. t.; Lee, Y. T.; Kung, A. H., *Review of Scientific Instruments* **1995**, *66* (10), 4841-4844.
28. Heimann, P. A.; Koike, M.; Hsu, C. W.; Blank, D.; Yang, X. M.; Suits, A. G.; Lee, Y. T.; Evans, M.; Ng, C. Y.; Flaim, C.; Padmore, H. A., *Review of Scientific Instruments* **1997**, *68* (5), 1945-1951.
29. Leone, S. R.; Ahmed, M.; Wilson, K. R., *Physical Chemistry Chemical Physics* **2010**, *12* (25), 6564-6578.
30. Stull, D. R., *Industrial & Engineering Chemistry* **1947**, *39* (4), 517-540.
31. Johnson, M.; Bodi, A.; Schulz, L.; Gerber, T., *Nuclear Instruments and Methods in Physics Research Section A: Accelerators, Spectrometers, Detectors and Associated Equipment* **2009**, *610* (2), 597-603.
32. Guan, Q.; Urness, K. N.; Ormond, T. K.; David, D. E.; Barney Ellison, G.; Daily, J. W., *International Reviews in Physical Chemistry* **2014**, *33* (4), 447-487.
33. Osborn, D. L.; Hayden, C. C.; Hemberger, P.; Bodi, A.; Voronova, K.; Sztáray, B., *The Journal of Chemical Physics* **2016**, *145* (16), 164202.
34. Sztáray, B.; Voronova, K.; Torma, K. G.; Covert, K. J.; Bodi, A.; Hemberger, P.; Gerber, T.; Osborn, D. L., *The Journal of Chemical Physics* **2017**, *147* (1), 013944.
35. Bodi, A.; Sztáray, B.; Baer, T.; Johnson, M.; Gerber, T., *Review of Scientific Instruments* **2007**, *78* (8), 084102.
36. Sztáray, B.; Baer, T., *Review of Scientific Instruments* **2003**, *74* (8), 3763-3768.
37. Montgomery, J. A.; Frisch, M. J.; Ochterski, J. W.; Petersson, G. A., *The Journal of Chemical Physics* **1999**, *110* (6), 2822-2827.
38. Montgomery, J. A.; Frisch, M. J.; Ochterski, J. W.; Petersson, G. A., *The Journal of Chemical Physics* **2000**, *112* (15), 6532-6542.
39. Frisch, M. J.; Trucks, G. W.; Schlegel, H. B.; Scuseria, G. E.; Robb, M. A.; Cheeseman, J. R.; Scalmani, G.; Barone, V.; Mennucci, B.; Petersson, G. A.; Nakatsuji, H.; Caricato, M.; Li, X.; Hratchian, H. P.; Izmaylov, A. F.; Bloino, J.; Zheng, G.; Sonnenberg, J. L.; Hada, M.; Ehara, M.; Toyota, K.; Fukuda, R.; Hasegawa, J.; Ishida, M.; Nakajima, T.; Honda, Y.; Kitao, O.; Nakai, H.; Vreven, T.; Montgomery, J. A.; Peralta, J. E.; Ogliaro, F.; Bearpark, M.; Heyd, J. J.; Brothers, E.; Kudin, K. N.; Staroverov, V. N.; Kobayashi, R.; Normand, J.; Raghavachari, K.; Rendell, A.; Burant, J. C.; Iyengar, S. S.; Tomasi, J.; Cossi, M.; Rega, N.; Millam, J. M.; Klene, M.; Knox, J. E.; Cross, J. B.; Bakken, V.; Adamo, C.; Jaramillo, J.; Gomperts, R.; Stratmann, R. E.; Yazyev, O.; Austin, A. J.; Cammi, R.; Pomelli, C.; Ochterski, J. W.; Martin, R. L.; Morokuma, K.; Zakrzewski, V. G.; Voth, G. A.; Salvador, P.; Dannenberg, J. J.; Dapprich, S.; Daniels, A. D.; Farkas, Ö.; Foresman, J. B.; Ortiz, J. V.; Cioslowski, J.; Fox, D. J., *Gaussian 09* **2009**.
40. da Silva, G., *Chemical Physics Letters* **2013**, *558* (0), 109-113.
41. Steinbauer, M.; Hemberger, P.; Fischer, I.; Bodi, A., *ChemPhysChem* **2011**, *12* (10), 1795-1797.
42. Traeger, J. C.; McLoughlin, R. G., *International Journal of Mass Spectrometry and Ion Physics* **1978**, *27* (4), 319-333.
43. Akai, N.; Kudoh, S.; Takayanagi, M.; Nakata, M., *Chemical Physics Letters* **2002**, *363* (5-6), 591-597.
44. Blanksby, S. J.; Ellison, G. B., *Accounts of Chemical Research* **2003**, *36* (4), 255-263.
45. Amouri, H.; Le Bras, J., *Accounts of Chemical Research* **2002**, *35* (7), 501-510.

46. Bai, W.-J.; David, J. G.; Feng, Z.-G.; Weaver, M. G.; Wu, K.-L.; Pettus, T. R. R., *Accounts of Chemical Research* **2014**, *47* (12), 3655-3664.
47. Eck, V.; Schweig, A.; Vermeer, H., *Tetrahedron Letters* **1978**, *19* (27), 2433-2436.
48. Bodi, A.; Hemberger, P.; Osborn, D. L.; Sztáray, B., *The Journal of Physical Chemistry Letters* **2013**, *4* (17), 2948-2952.
49. Krüger, J.; Garcia, G. A.; Felsmann, D.; Moshhammer, K.; Lackner, A.; Brockhinke, A.; Nahon, L.; Kohse-Höinghaus, K., *Physical Chemistry Chemical Physics* **2014**, *16* (41), 22791-22804.
50. Hemberger, P.; Custodis, V. B. F.; Bodi, A.; Gerber, T.; van Bokhoven, J. A., *Nature Communications* **2017**, *8*, 15946.
51. Cunha de Miranda, B. K.; Alcaraz, C.; Elhanine, M.; Noller, B.; Hemberger, P.; Fischer, I.; Garcia, G. A.; Soldi-Lose, H.; Gans, B.; Vieira Mendes, L. A.; Boyé-Péronne, S.; Douin, S.; Zabka, J.; Botschwina, P., *The Journal of Physical Chemistry A* **2010**, *114* (14), 4818-4830.
52. Holzmeier, F.; Herbert, M.-P.; Fischer, I.; Steglich, M.; Bodi, A.; Hemberger, P., *Journal of Analytical and Applied Pyrolysis* **2017**, *124*, 454-460.
53. Zhou, Z.; Xie, M.; Wang, Z.; Qi, F., *Rapid Communications in Mass Spectrometry* **2009**, *23* (24), 3994-4002.
54. Rosenstock, H. M.; Draxl, K.; Steiner, B. W.; Herron, J. T., Ion Energetics Data. In *NIST Chemistry WebBook, NIST Standard Reference Database Number 69*, Linstrom, P. J.; Mallard, W. G., Eds. National Institute of Standards and Technology: Gaithersburg MD, 20899, 2011.
55. Zador, J.; Huang, H.; Welz, O.; Zetterberg, J.; Osborn, D. L.; Taatjes, C. A., *Physical Chemistry Chemical Physics* **2013**, *15* (26), 10753-10760.
56. Ormond, T. K.; Hemberger, P.; Troy, T. P.; Ahmed, M.; Stanton, J. F.; Ellison, G. B., *Molecular Physics* **2015**, *113* (15-16), 2350-2358.
57. Parker, D. S. N.; Kaiser, R. I.; Troy, T. P.; Kostko, O.; Ahmed, M.; Mebel, A. M., *The Journal of Physical Chemistry A* **2015**, *119* (28), 7145-7154.
58. Lipert, R. J.; Colson, S. D., *The Journal of Chemical Physics* **1990**, *92* (5), 3240-3241.
59. Kobayashi, T.; Nagakura, S., *Bulletin of the Chemical Society of Japan* **1974**, *47* (10), 2563-2572.
60. Kobayashi, T., *Journal of Electron Spectroscopy and Related Phenomena* **1975**, *7* (4), 349-353.
61. Stanton, J. F.; Sattelmeyer, K. W.; Gauss, J.; Allan, M.; Skalicky, T.; Bally, T., *The Journal of Chemical Physics* **2001**, *115* (1), 1-4.
62. Ess, D. H.; Wheeler, S. E.; Iafe, R. G.; Xu, L.; Çelebi-Ölçüm, N.; Houk, K. N., *Angewandte Chemie International Edition* **2008**, *47* (40), 7592-7601.
63. Lee, T. J.; Taylor, P. R., *International Journal of Quantum Chemistry* **1989**, *36* (S23), 199-207.
64. Bezzina, J. P.; Prendergast, M. B.; Blanksby, S. J.; Trevitt, A. J., *The Journal of Physical Chemistry A* **2018**, *122* (4), 890-896.



Reactions of *ortho* and *meta*-methylphenyl radicals with oxygen form products that depend acutely on the position of the methyl group